ACS Catalysis

Research Article

pubs.acs.org/acscatalysis

Ligand Scaffold Optimization of a Supramolecular Hydrogenation Catalyst: Analyzing the Influence of Key Structural Subunits on Reactivity and Selectivity

Nathan C. Thacker, Shin A. Moteki,† and James M. Takacs*

Department of Chemistry, University of Nebraska-Lincoln, Lincoln, Nebraska 68588-0304, United States

Supporting Information

ABSTRACT: Results are reported for the catalytic asymmetric hydrogenation of two prototypical substrates with a series of more than 150 closely related supramolecular catalysts differing in only their ligand/catalyst scaffold. These modular catalysts are constructed from four subunits and vary widely in their reactivity (no reaction to quantitative yield) and enantioselectivity (racemic to 96% enantiomeric excess (ee)). Analysis of the ligand/catalyst scaffold optimization data reveals how each subunit contributes to the effectiveness of the modular supramolecular catalyst. The results suggest that a balance between key elements of rigidity and flexibility is required for the successful catalysts and, moreover, that this balance is required to enable effective fine-tuning via catalyst scaffold optimization.

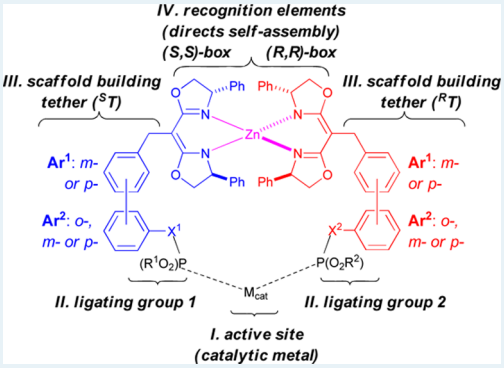

KEYWORDS: *supramolecular catalysis, asymmetric catalysis, asymmetric hydrogentaion, self-assembled ligands, self-assembly, rhodium-catalyzed*

INTRODUCTION

Asymmetric catalysis using chiral metal complexes brings into focus the prominent roles played by chiral ligands. It is the coordinated ligand assembly that is expected to sculpt the topography creating a "chiral catalytic pocket" around the catalytic metal center, which in turn directs the stereochemical course of the catalyzed bond construction. At the same time, the ligand(s) must impart the appropriate characteristics at the metal center to promote reactivity. The successful use of DIPAMP in the early days of rhodium-catalyzed asymmetric hydrogenation defined the strategy of covalently linking chiral ligating groups to organize chirality while exploiting C_2-symmetry to define an effective topography via relatively small, rigid metal chelates.[1−3] At the time, this approach proved much more successful than the alternative use of two equivalents of a similar monodentate ligand (i.e., PAMP). It has been subsequently shown that appropriately chosen monodentate ligands, presumably ones for which nonbonded interactions between the coordinated ligands restrict their relative orientation and thereby organize the chiral pocket for catalysis, can also give very effective catalyst systems.[4−8] These two, now standard, approaches to organizing chirality at the site of catalysis (i.e., M_{cat}) are illustrated schematically by structures **1** and **2** (Figure 1). Their success raises the question, what other approaches can be exploited to organize the chiral ligating groups and create the topography needed for efficient new catalyst systems?[9]

Hydrogen bonding and metal complexation are common structural motifs used in nature to direct the three-dimensional assembly of a protein framework so as to position the active site functionalities and create the chiral pocket for biocatalysts.[10] We and others are exploring the use of these strategies to organize chirality and define the topography for supramolecular chemocatalysts[11−18] building on the studies of supramolecular chemistry,[19−26] especially in the context of ligands and organometallic catalysts constructed via self-assembly whether by metal complexation,[27−34] hydrogen bonding[35−46] or nonbonded interactions.[47] The concept is illustrated schematically by the bimetallic catalyst (i.e., structure **3**) shown in Figure 1.

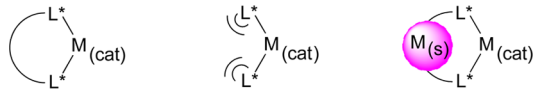

Figure 1. Organizing chirality (i.e., L*) via a short covalent tether (**1**), nonbonded interactions (**2**), and metal complexation (**3**, M_S represents a metal complex whose role is principally structural).

Among the fundamental questions underpinning investigations into supramolecular catalyst systems are whether such strategies can be used to give effective catalysts, for example, asymmetric catalysts, and whether the strategies employed to prepare such catalysts offer advantages over the traditional approaches. One potential advantage offered by self-assembled

Received: July 12, 2012
Revised: November 1, 2012
Published: November 5, 2012

systems is that combinatorial methods can be exploited to facilitate ligand/catalyst synthesis. Another is the potential to fine-tune catalyst performance in ways not as readily available with the traditional approaches. However, many challenges remain. Among these, one finds that while significant progress has been made toward understanding how to optimize catalyst performance using the classical small-molecule catalyst motifs,[48,49] other than the design of efficient screening protocols,[50,51] much less is known about how to optimize the performance of supramolecular catalysts. The present study of ligand/catalyst scaffold optimization analyzes data obtained from the rhodium-catalyzed asymmetric hydrogenations of two prototypical enamide substrates to illustrate how each subunit of the modular supramolecular catalyst contributes to its effectiveness.

RESULTS AND DISCUSSION

The heterobimetallic complex **4** (Figure 2) defines a series of self-assembled supramolecular catalysts. Catalysts based on this

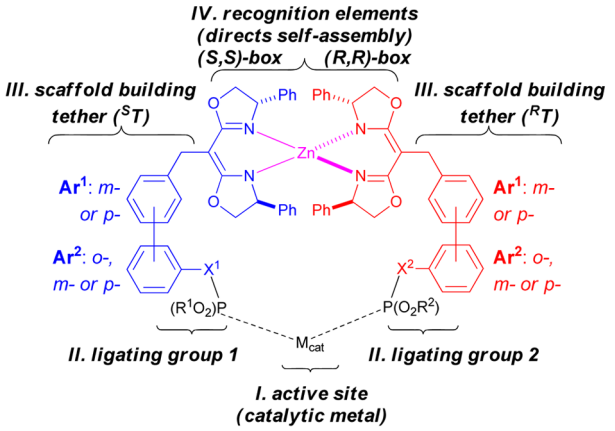

modular supramolecular catalysts [Zn(ST,RT)]Mcat (4)

	X = O		X = CH_2O	
Ar^2	1,3-Ar^1	1,4-Ar^1	1,3-Ar^1	1,4-Ar^1
-	A	B	I	J
1,2-	C	D	K	L
1,3-	E	F	M	N
1,4-	G	H	O	P

Figure 2. General structure representing a series of heterobimetallic supramolecular catalysts **4** derived from SALs **Zn(ST RT)** in which combinations of tethers ST and RT (ST,RT = A–P) generate a collection of structurally related ligand scaffolds.

design have previously been used for efficient asymmetric allylic amination[52] and catalytic asymmetric hydroboration.[53,54] These complexes incorporate one metal (i.e., Zn(II)), whose key role is presumably only structural, and a second metal, designated M_{cat}, whose key role is to catalyze the desired reaction. Structure **4** is modular in its design and composed of four subunits: an active site (subunit I); ligating groups (subunit II); scaffold-building tethers (subunit III); and recognition elements (subunit IV). Chiral bisoxazolines (box) serve as the recognition elements to direct self-assembly via chiral discrimination. That is, box subunits of complementary chirality combine with Zn(II) to form the thermodynamically favored heteroleptic complex with high selectivity (Figure 3).[55,56] Each box moiety bears a variable scaffold-building tether (ST and RT)

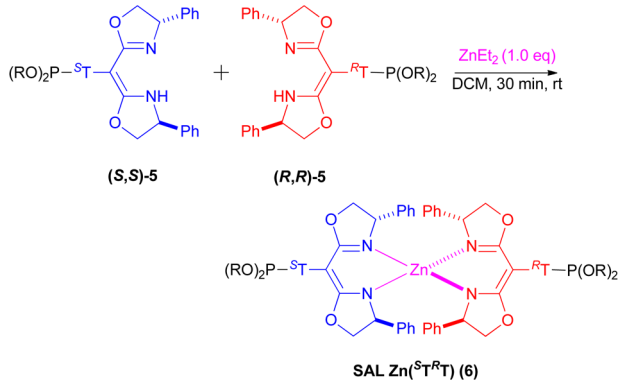

Figure 3. Addition of $ZnEt_2$ to an equimolar mixture of (*S*,*S*)-**5** and (*R*,*R*)-**5** leads to formation of the heteroleptic complex SAL **Zn(STRT)**.

consisting of an aryl or biaryl ring whose structure is further varied by the ortho-, meta-, or para-substitution pattern of those rings. Each tether is terminated by an aryloxy (ArO-, tethers **A**–**H**) or a hydroxymethyl group ($ArCH_2O$-, tethers **I**–**P**).

The hydroxyl functionalities residing in tethers ST and RT serve as convenient attachment points for the ligating group subunits. In doing so, combining (*S*,*S*)- and (*R*,*R*)-box derivatives bearing chiral phosphite terminated tethers **A**-**P** (i.e., assembling the recognition, scaffold-building and ligating group subunits) enables the facile preparation of hundreds of chiral bidentate, self-assembled ligands (i.e., SAL **Zn(STRT)**) differing in the combination of scaffold-building tethers, ST and RT.[57] The metal ultimately responsible for catalysis, M_{cat}, is the active site subunit. Combining M_{cat} with each SAL **Zn(STRT)** affords a series of supramolecular catalysts **4**, each possessing a different catalyst scaffold. In the present study of asymmetric hydrogenation, the ligating group is restricted to a chiral phosphite (principally, the BINOL-dervied phosphite) and the catalytic metal limited to Rh(I) (for the most part as its tetrafluoroborate salt).

The supramolecular catalysts defined by structure **4** offer the potential to tune catalyst activity by making a large number of subtle changes to the ligand/catalyst scaffold, an approach that typically is challenging using the more traditional approaches to catalyst design in Figure 1. A preliminary investigation into rhodium-catalyzed asymmetric hydrogenations (CAH) of dehydroaminoacid derivatives using a series of SALs bearing chiral (*R*)-5,5′,6,6′-tetramethylbiphenyl-2,2′-diol (BIPHEP) derived phosphite ligating groups, that is, (BIPHEP)SAL **Zn(STRT)**, was previously reported.[58] Herein, we focus on results obtained using in situ generated (BINOL)SAL **Zn-(STRT)** ligands in combination with $Rh(nbd)_2BF_4$ for the rhodium-catalyzed asymmetric hydrogenations of two prototypical substrates, **S1** and **S2** (Figure 4).[59] Analysis of the data reveals the extent to which each catalyst subunit influences the efficiency of the supramolecular catalyst.

Influence of the Ligating Group Subunit. As expected, the nature of the ligating group (i.e., **4**, subunit II) directly bound to the site of reaction plays a very important role in determining the catalyst efficiency. The phenyl and benzyl monophosphites derived from TADDOL, BIPHEP, and BINOL diols (i.e., **L1a/b**–**L3a/b**) can be thought of as simplified, unconstrained model ligands for comparison to the corresponding SAL-derived supramolecular catalyst systems **4**.

dx.doi.org/10.1021/cs300465u | ACS Catal. 2012, 2, 2743–2752

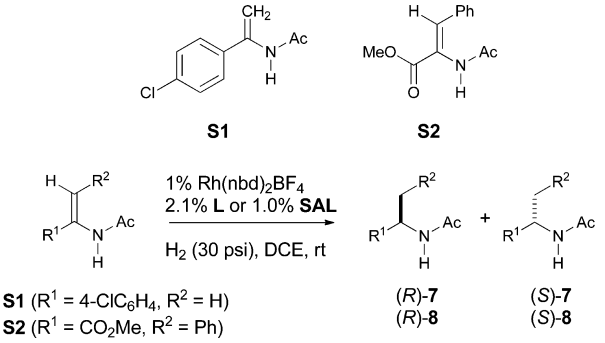

Figure 4. General conditions employed for rhodium-catalyzed asymmetric hydrogenation of two prototypical substrates.

In particular, the phenyl phosphites serve as models for the SALs derived from subunits **A**–**H**, benzyl phosphites for those SALs incorporating tether subunits **I**–**P**. Hydrogenation of **S1** and **S2** (Table 1) using the (*R*)-TADDOL-derived mono-

Table 1. Rhodium-Catalyzed Asymmetric Hydrogenation of S1 and S2 Using Model Phosphite Ligands[a]

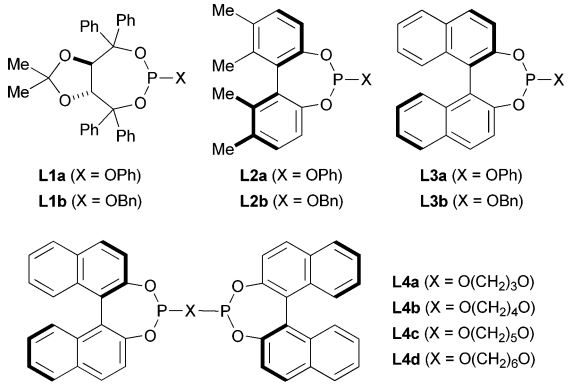

		S1		S2	
entry	ligand	ee (%)[b]	yld (%)	ee (%)[b]	yld (%)
1	**L1a**	10	99	4	97
2	**L1b**	15	99	30	99
3	**L2a**	67	99	67	99
4	**L2b**	53	99	53	65
5	**L3a**	86	99	69	99
6	**L3b**	92	99	78	99
7	**L3a** + **L3b**[c]	92	99	78	99
8	**L4a**	26	93	20	99
9	**L4b**	68	90	87	99
10	**L4c**	64	87	71	99
11	**L4d**	43	99	13	90

[a]Reaction conditions: 1 mol % $Rh(nbd)_2BF_4$, 2.1 mol % monophosphite, or 1.0 mol % SAL **Zn**(^{S}**T**^{R}**T**), H_2 (30 psi), DCE, rt, 16 h. Yields and enantioselectivity determined by chiral GC using *N*-benzylacetamide as an internal standard. [b]Unless otherwise noted, the (*S*)-enantiomer predominates in the reaction. [c]Equimolar amounts of each ligand.

phosphites (i.e., **L1a** and **b**) give only low levels of enantioselectivity under the conditions shown above (4–30% ee, Table 1 entries 1 and 2). The corresponding (*R*)-BIPHEP derivatives give moderate levels of enantioselectivity, 53–67% ee (entries 3 and 4) with the phenyl phosphite **2a** giving higher selectivity. The (*R*)-BINOL phosphites **L3a** and **b** give still higher levels of enantioselectivity (69–92% ee), and in each case, the reaction affords near quantitative yield of the hydrogenated product (entries 5 and 6).[60] The BINOL phosphites, however, are more successful with substrate **S1** than with **S2**, and in contrast to the BIPHEP derivatives, the BINOL-derived benzyl phosphite **L3b** affords higher enantiomeric excess (ee) than the phenyl phosphite **L3a**. For the purpose of comparison to the results obtained with certain of the SALs presented below, it should be noted that the mixed ligand combination,[61,62] that is, using equimolar amounts of **L3a** and **L3b**, gives 92% and 78% ee for substrates **S1** and **S2**, respectively.

The chiral monodentate ligands discussed above provide benchmarks for the effectiveness of chiral phosphite ligating groups lacking any connecting scaffold. To benchmark the effectiveness of a relatively nonstructured ligand scaffold, a series of BINOL-bisphosphites (**L4a**–**d**) were prepared from 1,n-diols.[63] These simple bisphosphites, spaced by 3 to 6 methylene units, varied widely in their effectiveness. Enantioselectivity ranged from 26–68% ee for the reactions of **S1** and from 13–87% ee for the reaction of **S2** (entries 8–11). Only one combination, the reaction of **S2** using the 1,4-butane diol derived **L4b**, gives product in higher enantiomeric excess, albeit only incrementally higher, than the best monophosphite, that is, 87% versus 78% ee (Table 1, compare entry 9 to entry 6).

BINOL-bisphosphite SALs, that is, (BINOL)SAL **Zn**(^{S}**T**^{R}**T**), were prepared from combinations of tether subunits **A**–**P** by treating the appropriate (*S*,*S*)- and (*R*,*R*)-**5** box derivatives with Et_2Zn.[64] Each SAL was subsequently combined with $Rh(nbd)_2BF_4$ to effect the in situ preparation of over 165 closely related supramolecular catalysts, each bearing the same two (BINOL)P-ligating groups but differing in the catalyst scaffold. The results obtained as a function of scaffold are discussed in detail below. However, among the scaffolds tested, (BINOL)SAL **Zn(IC)** affords the highest level of enantioselectivity for both **S1** and **S2**, giving 96% and 93% ee, respectively (Table 2, entry 3). These levels of enantiomeric excess are higher than those obtained using **L3a** (**S1** 86% ee; **S2** 69% ee), **L3b** (**S1** 92% ee; **S2** 78% ee) or any obtained using the bisphosphites bearing flexible scaffolds, that is, **L4a**–**d** (Table 1, entries 8–11). (BINOL)SAL **Zn(IC)** contains one benzyl-like ($ArCH_2O$-linked) phosphite and one phenyl-like (ArO-linked) phosphite within its structure and thus, the mixed combination of monophosphites **L3a**/**b** (Table 1 entry 7, **S1** 92% ee; **S2** 78% ee) is perhaps the most relevant performance benchmark for comparison.[65]

Table 2 compares the results obtained using (TADDOL)SAL **Zn(IC)** (entry 1) and (BIPHEP)SAL **Zn(IC)** (entry 2) to those obtained with (BINOL)SAL **Zn(IC)** (entry 3). The results demonstrate the significance of the ligating group on the performance of the supramolecular catalyst. The TADDOL- and BIPHEP-derived SALs with the same catalyst scaffold exhibit low reactivity and only low levels of enantioselectivity. The differences between the performance of (BIPHEP)SAL **Zn(IC)** and (BINOL)SAL **Zn(IC)** are particularly striking and surprising in light of the structural similarities of the two ligating groups and the results obtained with monophosphites **L2a** and **L3a**. In contrast, (BIPHEP)SAL **Zn(IC)** and (BINOL)SAL **Zn(IC)** differ significantly in terms of yield (21–76% versus 99%) and enantioselectivity (23–25% ee versus 93–96% ee). The truncated models of (BINOL)SAL **Zn(IC)**, **L5** and **L6**, serve as control experiments showing that the ligating group alone is not sufficient for optimal

dx.doi.org/10.1021/cs300465u | *ACS Catal.* 2012, 2, 2743–2752

Table 2. Influence of the Ligating Group on the Performance of SAL Scaffold Zn(IC)[a]

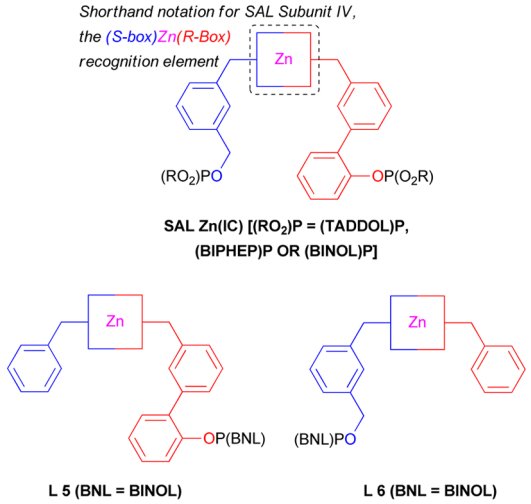

entry	ligand	S1 ee (%)	yld (%)	S2 ee (%)	yld (%)
1	(TADDOL)SAL **Zn(IC)**	31	68		NR
2	(BIPHEP)SAL **Zn(IC)**	23	76	25	21
3	(BINOL)SAL **Zn(IC)**	96	99	93	99
4	**L5** (2.1 equiv)	65	13	30	2
5	**L6** (2.1 equiv)	92	99	85	99

[a]Reaction conditions: 1 mol % $Rh(nbd)_2BF_4$, 1.0 mol % SAL **Zn**(^{S}**T**^{R}**T**) or 2.1 mol % monophosphite, H_2 (30 psi), DCE, rt, 16 h. Yields and enantioselectivity determined by chiral GC using *N*-benzylacetamide as an internal standard. Unless otherwise noted, the (*S*)-enantiomer predominates.

performance. Note that the results obtained with **L6** are essentialy the same as those obtained using **L3b** (see Table 1).

In summary, since the ligating group is the chiral element directly bound to rhodium and closest to the reacting substrate, its critical importance in determining reactivity and selectivity is of course expected. The yield and enantioselectivity data comparing mono- to bisphosphites show that a conformationally mobile tether (**L4a**−**L4d**) is usually detrimental compared to the monophosphite and only occasionally results in comparable or modestly enhanced catalyst performance. While catalyst efficiency was found to be optimized with a more highly structured bisphosphite scaffold (i.e., (BINOL)SAL **Zn(IC)**), the high levels of reactivity and selectivity are intimately tied to the combination of scaffold and ligating group. Attaching other ligating groups to the same scaffold do not necessarily enhance catalyst performance over that of the corresponding monophosphites; this is shown to be the case with TADDOL- and BIPHEP-derived bisphosphites.

Influence of the Ligand/Catalyst Scaffold. The various tether subunits shown in Figure 1 were combined with Et_2Zn and $Rh(nbd)_2BF_4$ to effect the in situ preparation of 169 closely related supramolecular (BINOL)SAL **Zn**(^{S}**T**^{R}**T**) catalysts. Each supramolecular catalyst bears the same two (BINOL)P-ligating groups but differ in the ligand/catalyst scaffold. Each catalyst was screened individually in the asymmetric hydrogenation of substrate **S1** under a standard set of reaction conditions. The data are analyzed in several ways as discussed in the paragraphs that follow.

The plot in Figure 5 compiles the stereochemical results; these data are simply sorted from low levels of enantioselectivity to high without regard to scaffold structure. As discussed above, the most selective catalyst, (BINOL)SAL **Zn(IC)**, affords *S*-**2a** in 96% ee. The plot can be divided into three regions: (1) a flat region representing a group of approximately 11 catalysts that afford racemic product; (2) a group of roughly 50 catalysts whose performance spans a wide range from racemic to greater than 80% ee; and (3) a large plateau region composed of data for 106 catalysts whose behavior varies within a relatively narrow range (87−96% ee). Thus, the effects of subtle differences in the structure of the catalyst scaffold run the entire range, some markedly influence catalyst selectivity while the effects of others are only incremental.

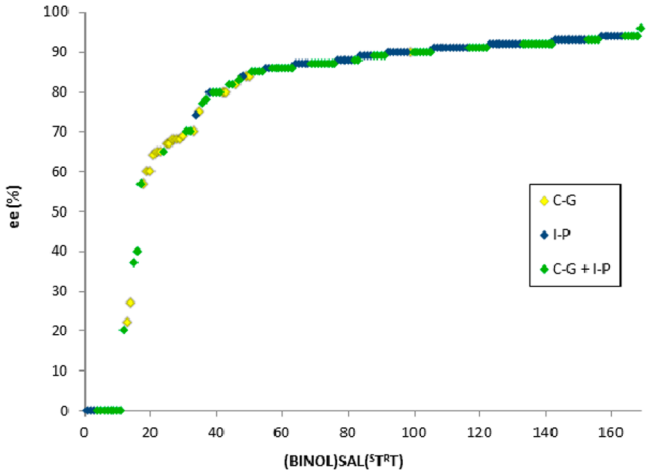

Figure 5. Observed enantioselectivity for the CAH of **S1** sorted from high to low as a function of catalyst scaffold (BINOL)SAL **Zn**(^{S}**T**^{R}**T**). The yellow data points incorporate only tethers **C**−**G**, the blue only **I**−**P**, and the green for mixed combinations of (**C**−**G**) with (**I**−**P**).

The data in Figure 5 can be further analyzed in terms of scaffold structure. The individual data points in Figure 5 are color coded. Those highlighted in yellow represent supramolecular catalyst scaffolds incorporating only tethers **C**−**G** (that is, only ArO-P(BINOL) linkages), those in blue only **I**−**P** (i.e., only $ArCH_2O$−P(BINOL) linkages), and those in green represent mixed combinations of (**C**−**G**) with (**I**−**P**). Looking more closely at the data, the yellow data points tend to cluster toward the low end of the percent enantiomeric excess range. Only a few scaffolds containing only combinations of ArO-linkages to the BINOL-phosphite ligating group are as selective as the model phenyl monophosphite **3a**. Thus, it seems that the constraints imposed by the scaffold detract from the effectiveness of the ligating group for these derivatives. On the other hand, supramolecular catalysts bearing only $ArCH_2O$-linkages (the blue data points) tend to dominate the high end plateau region; that is, they show little variation in performance as a function of the catalyst scaffold. The observed enantioselectivities for those catalysts are rather tightly clustered around that obtained with the model benzyl monophosphite **3b**. The green data points representing mixed ArO- and $ArCH_2O$-linkages are spread more evenly throughout the range of catalyst performance, from racemic to 96% ee.

In screening the supramolecular catalysts, all reactions are run under a standard set of reaction conditions, and in addition to R/S ratios, the product yield was determined by comparison to an internal GC standard. Not all catalysts effect complete

dx.doi.org/10.1021/cs300465u | *ACS Catal.* 2012, 2, 2743−2752

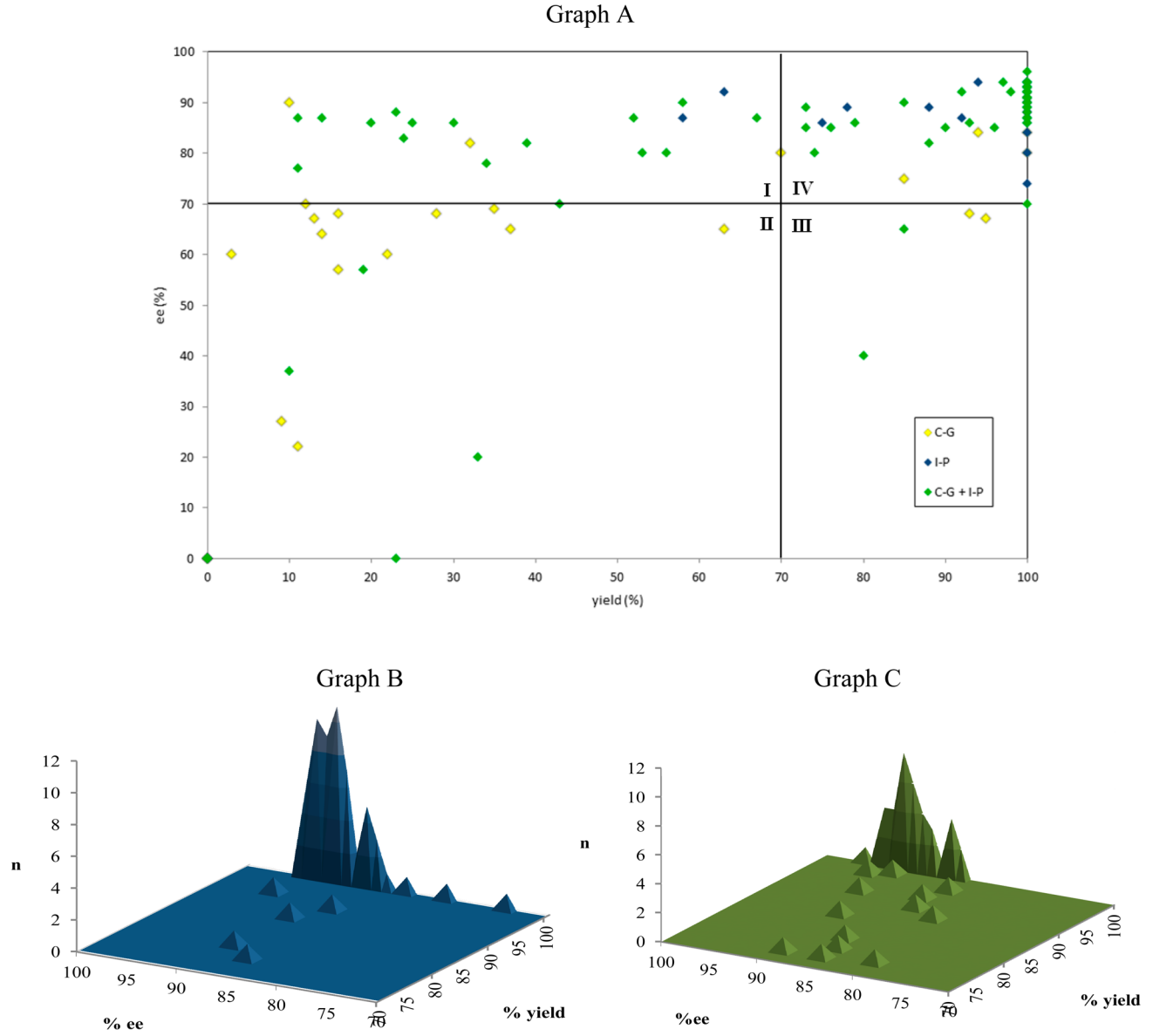

Figure 6. Plot of catalyst performance (% ee versus % yield) in the CAH of **S1** coded by tether combination: Graph A, overall data set for all catalysts screened (note that some points are obscured by overlapping data); Graph B, Quadrant IV data only (% ee and % yield greater than 70%) for all catalysts combinations of only tethers **I**–**P**; and Graph C, Quadrant IV data only (% ee and % yield greater than 70%) for catalysts combinations of tethers **C**–**G** with tether **I**–**P**.

consumption of starting material under the conditions employed indicating their relatively low reactivity or susceptibility toward catalyst inactivation. This is in stark contrast to the quantitative conversion observed using BINOL monophosphite ligands **L3a**–**L3b** (Table 1, entries 5–6). Plotting percent enantiomeric excess versus percent yield shows that catalyst turnover is also systematically affected by the scaffold structure (Figure 6).[66] Graph A summarizes all of the data with the individual data points again color coded by tether combination. The upper right-hand quadrant (labeled IV) represents catalysts for which the yield and enantioselectivity are 70% or greater. This perspective of the data reveals a number of interesting trends. First, the high yield-high enantioselectivity quadrant IV is rather densely populated. Nonetheless, a significant number of catalysts, as represented in the upper left-hand quadrant I, give relatively high enantiomeric excess but only moderate-to-low yield. That is, a number of catalysts are quite selective but exhibit slow turnover or are prone to deactivation. In contrast, relatively few catalysts populate the lower right-hand quadrant III, that is, catalysts that exhibit average or better turnover frequency but low enantioselectivity.[67]

Focusing on the ArO- or $ArCH_2O$-linkage within each catalyst, data in Figure 6 show that catalyst scaffolds containing only ArO-phosphite linkages (i.e., yellow data points) tend to be more highly represented among those catalysts giving lower yield, lower enantioselectivity, or both (quadrant II). In contrast, few blue data points, that is, those representing only $ArCH_2O$-phosphite linkages, lie outside the high yield-high enantioselectivity quadrant. Those catalysts containing a combination of ArO- and $ArCH_2O$-linkages, represented by the green data points, tend to be quite varied in their performance.

dx.doi.org/10.1021/cs300465u | *ACS Catal.* 2012, 2, 2743–2752

The smaller plots within Figure 6 give separate expanded stack plots for the high yield-high enantioselectivity quadrant IV catalysts; only $ArCH_2O$-linkage data are shown in Graph B with the mixed linkage data presented in Graph C. These views support the conclusion that the performance of mixed-linkage catalysts is more sensitive to the precise structure of the scaffold while the benzyl-only linked catalysts are not as readily fine-tuned by scaffold modification. One possible explanation for the difference between the $ArCH_2O$-only linkage and mixed linkage catalysts is that, aside from subtle electronic differences, the additional degree of rotational freedom afforded to the former tends to work against subtle structural changes in the scaffold translating to measurable changes in the chiral topography.

Having examined overall trends in the data summarized above, Figure 7 highlights the empirically identified "best"

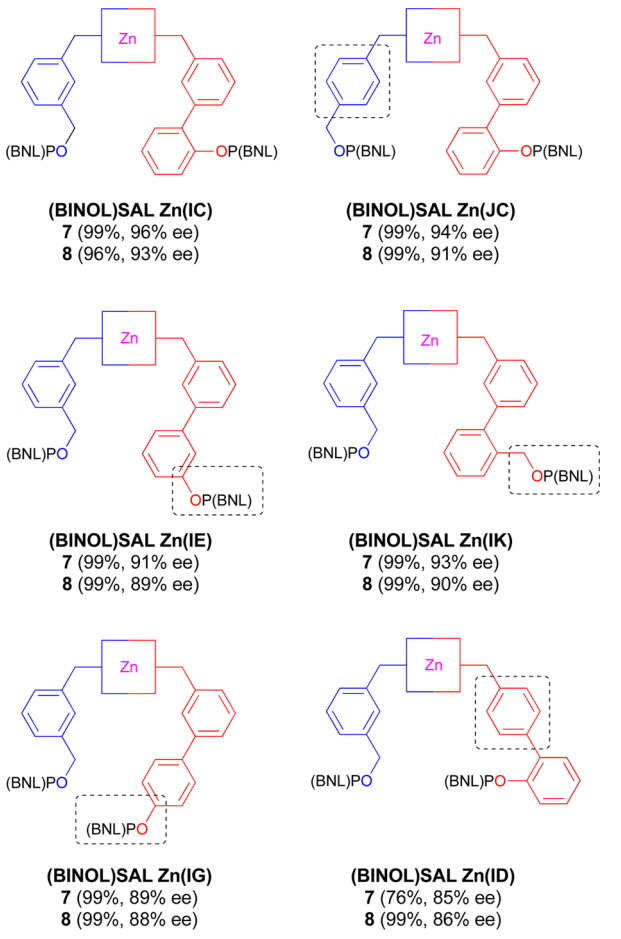

Figure 7. Illustrating the largely incremental effect of varying the structure of the empirically determined optimal catalyst scaffold.

scaffold structure, (BINOL)SAL **Zn(IC)**, and how subtle structural changes effect catalyst performance. Having arrived at a structural "sweet-spot" with (BINOL)SAL **Zn(IC)**, it is perhaps somewhat surprising to find that subtle changes to that structure result in only small changes in catalyst performance. For example, comparing (BINOL)SAL **Zn(IC)** to the isomeric (BINOL)SAL **Zn(JC)** or to the one-carbon-homologated (BINOL)SAL **Zn(IK)**, one finds little change in catalyst performance; the observed yields (99%) and enantioselectivity (93−96% ee and 90−93% ee for substrates **S1** and **S2**, respectively) remain high for each catalyst. Other structural changes have a somewhat more significant, albeit still incremental, effect. The isomeric SALs in which the phenyl phosphite linkage is 1,3 or 1,4 (i.e., (BINOL)SAL **Zn(IE)** and (BINOL)SAL **Zn(IG)**) rather than 1,2 as in (BINOL)SAL **Zn(IC)**, or when the arene attached to the box moiety is 1,4 rather than 1,3 (i.e., (BINOL)SAL **Zn(ID)** all afford somewhat less efficient catalysts (i.e., 85−91% ee and 86−89% ee for substrates **S1** and **S2**, respectively).

Table 3 compares a more extensive set of structures differing in the 1,2-, 1,3-, and 1,4-substitution pattern defining (*S*,*S*)-**5**

Table 3. Relatively Small Changes in the Structure of a Large Supramolecular Catalyst Can in Some Cases Significantly Influence the Reactivity and Enantioselectivity in the CAH of S1[a]

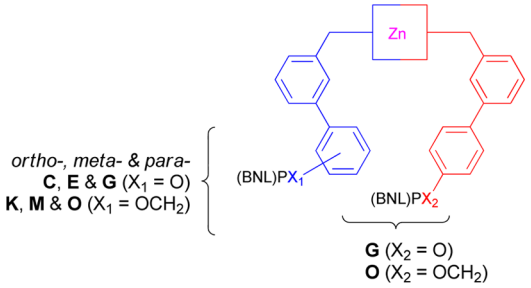

entry	(BINOL)SAL Zn(^{S}T^{R}T)	X_1	X_2	ee (%)[b]	yld (%)
1	**CG**	O	O	60	22
2	**EG**	O	O	68	28
3	**GG**	O	O	67	95
4	**KG**	CH_2O	O	85	90
5	**MG**	CH_2O	O	82	88
6	**OG**	CH_2O	O	94	99
7	**CO**	O	CH_2O	70	99
8	**EO**	O	CH_2O	87	99
9	**GO**	O	CH_2O	93	99
10	**KO**	CH_2O	CH_2O	89	88
11	**MO**	CH_2O	CH_2O	89	78
12	**OO**	CH_2O	CH_2O	93	99

[a]Reaction conditions: 1 mol % $Rh(nbd)_2BF_4$, 1.0 mol % (BINOL)SAL **Zn**(^{S}T^{R}T), H_2 (30 psi), DCE, rt, 16 h. Yields and enantioselectivity determined by chiral GC using *N*-benzylacetamide as an internal standard. [b]Unless otherwise noted, the (*S*)-enantiomer predominates in the reaction.

(i.e., ^{S}T) coupled with two closely related subunits defined by (*R*,*R*)-**5** (i.e., ^{R}T = G and O). The Table compares data for catalysts incorporating only ArO-linkages (entries 1−3), mixed combinations (entries 4−9), and only $ArCH_2O$-linkages (entries 10−12). Within this series we see considerably more variation in catalyst performance, yet the data otherwise tend to reinforce the trends discussed above. Catalysts bearing only ArO- linkages (entries 1−3) tend to give lower enantioselectivity and a wider range of yield than other combinations. For example, compare entries 1−3 (60−68% ee, 22−95% yield) to entries 4−9 (70−94% ee, 88−99% yield) and entries 10−12 (88−93% ee, 78−99% yield).

Examining the data in Table 3 in more detail reveals interesting contrasts. Compare the results obtained with (BINOL)SAL **Zn(OG)** (entry 6, 94% ee, 99% yield) to two close analogues. (BINOL)SAL **Zn(GG)** differs in structure by the absence of just one methylene unit but is decidedly less enantioselective (entry 3, 67% ee, 95% yield). In contrast, its

dx.doi.org/10.1021/cs300465u | *ACS Catal.* 2012, 2, 2743−2752

homologue (BINOL)SAL **Zn(OO)** differs by the inclusion of one additional methylene unit and performs nearly the same as the optimal catalyst (entry 12, 93% ee, 99% yield).

In summary, as suggested above in the discussion on the influence of the ligating group, the precise structure and nature of the tether subunit can play an important role in the efficiency of the reaction catalyzed by these supramolecular catalysts. Subtle structural changes can, but do not always, have a big effect on enantioselectivity, yield, or both. The data suggest that a balance between key elements of rigidity and flexibility is required for the successful catalysts and, moreover, that balance is required to enable effective fine-tuning via catalyst scaffold optimization.[68] Without sufficient rigidity, subtle changes in the scaffold structure are relatively ineffective for catalyst optimization; the same holding true in cases lacking sufficient flexibility.

Perhaps the most surprising finding is that for the systems studied, subtle changes around the empirically determined "structural sweet spot" tend to have only small incremental effects on catalyst performance. This may reflect the capacity of a macrocyclic chelate to accommodate small changes in structure without requiring significant changes to its overall three-dimensional shape.

Influence of the Recognition Element Subunit. The nominal structures of all supramolecular catalysts examined in this study are quite similar by design, and many are isomeric with one another by virtue of subtle differences in tether subunit substitution patterns. However, only a subset of structures differ in one rather subtle way involving the recognition element subunit rendering them diastereomeric. For example, consider the structures of (BINOL)SAL **Zn(OG)** and (BINOL)SAL **Zn(GO)** generated from combinations of (*S*,*S*)-**5O** with (*R*,*R*)-**5G** and (*S*,*S*)-**5G** with (*R*,*R*)-**5O**, respectively. These ligands differ only by the interchange of the two tether subunits appended to the box-zinc complex. The core ((*S*,*S*)-box)Zn(*R*,*R*-box) recognition subunit that directs heteroleptic self-assembly has the element of inversion symmetry.[55]That symmetry element is lost when chiral ligating groups are appended to the core. Consequently, (BINOL)SAL **Zn(OG)** and (BINOL)SAL **Zn(GO)** are diastereomers. Their derived supramolecular catalysts therefore need not exhibit the same reactivity or selectivity; however, the box substituents are seemingly far removed from the site of catalysis (i.e., the Rh center), and we initially assumed any difference in catalyst performance would be insignificant.

It indeed often proves to be the case that similar reactivity and selectivity is exhibited by pairs of diastereomeric catalysts. For example, the diastereomeric (BINOL)SAL **Zn(OG)**- and (BINOL)SAL **Zn(GO)**-derived catalysts give nearly identical results ((see Table 3, entries 6 and 9: quantitative yield, 93−94% ee). However, this is not always the case; for example, (BINOL)SAL **Zn(IC)** and its diastereomer (BINOL)SAL **Zn(CI)** (Figure 8) exhibit quite different catalyst performance, 96% versus 87% ee. The graph in Figure 8 plots the well-known relationship between percent enantiomeric excess and the difference in activation energies for the reactions leading to (*S*)- and (*R*)-products (i.e., $\Delta\Delta G^{\ddagger}$(S/R)). For the catalysts derived from (BINOL)SAL **Zn(IC)** and (BINOL)SAL **Zn(CI)**, the difference in enantioselectivity (Δes) translates to an estimated 0.73 kcal/mol [difference in ($\Delta\Delta G^{\ddagger}$(R/S))] for the diastereomeric catalysts.

In addition to differences in enantioselectivity, some pairs of diastereomeric catalysts exhibit significant differences in the chemical yield obtained under the standard reaction conditions suggesting significant differences in catalyst turnover rates and/or catalyst deactivation. Figure 9 plots the difference in enantioselectivity (Δes, expressed in kcal/mol) versus the increase or decrease in percent yield for the 78 pairs of diastereomeric catalyst combinations evaluated.

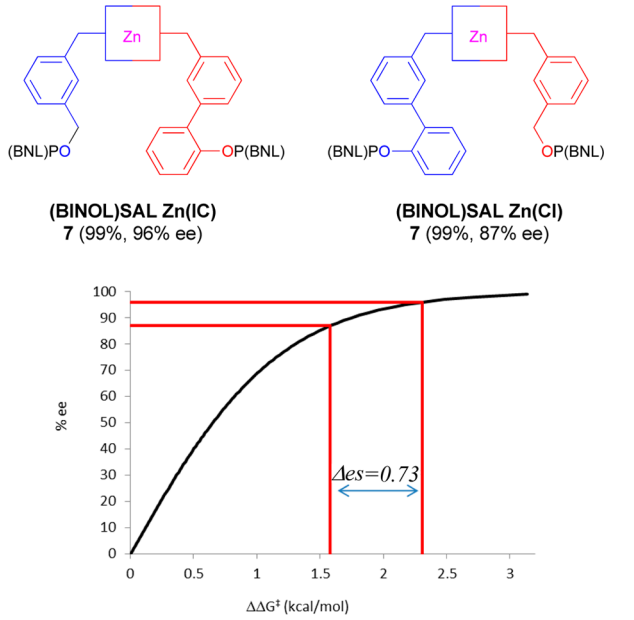

Figure 8. Theoretical relationship between enantioselectivity and the difference in ($\Delta\Delta G^{\ddagger}$ (R/S)); diastereomeric catalysts can afford a large difference in enantioselectivity defined as Δes.

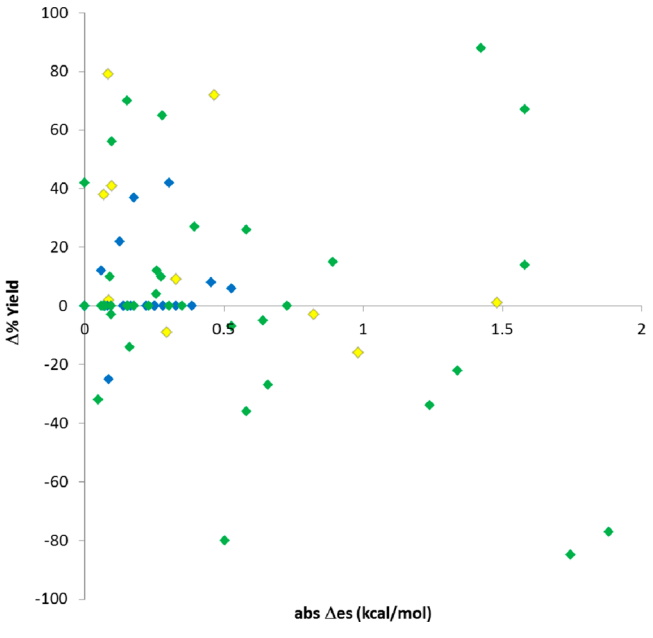

Figure 9. Differences in yield and enantioselectivity between 78 pairs of diastereomeric catalysts in the CAH of **S1**, (BINOL)SAL **Zn**(^{S}**T**^{R}**T**), as revealed by a plot of Δes (kcal/mol) versus the increase or decrease in percent yield obtained for the more selective of the diastereomeric catalysts. The yellow points incorporate only tethers **C**−**G** in the catalyst scaffold, the blue only **I**−**P**, and the green are for mixed combinations of (**C**−**G**) with (**I**−**P**).

dx.doi.org/10.1021/cs300465u | *ACS Catal.* 2012, 2, 2743−2752

Most diastereomeric catalysts, especially those bearing only $ArCH_2O$-linkages (data in blue), exhibit relatively small differences in enantioselectivity and yield. This is consistent with the idea that in most cases the box moieties exert little influence on what occurs at the site of reaction (i.e., at rhodium). However, others show rather striking matched/mismatched behavior suggesting that the recognition subunit along with the tethers that make up the catalyst scaffold significantly impact catalyst efficiency. This is especially true for scaffolds bearing mixed phenyl/benzyl linkages (data in green) and to a lesser extent those bearing only phenyl-type linkages (data in yellow). The data also suggest that increased enantioselectivity is more frequently accompanied by improved rather than diminished yield when comparing these diastereomeric catalyst pairs.

Data for several of the more striking cases of matched/mismatched behavior are summarized in Table 4. (BINOL)SAL

Table 4. Several Striking Cases in Which Pairs of Diastereomeric (BINOL)SAL Zn(^{S}T^{R}T) Catalysts Exhibit Matched/Mismatched Reactivity and/or Enantioselectivity in the CAH of Substrate of S1[a]

entry	Zn (^{S}T^{R}T)	%ee (% yld)	Zn (^{S}T^{R}T)	%ee (% yld)	Δes (kcal/mol)
1	**OG**	94 (99)	**GO**	93 (99)	0.09
2	**IC**	96 (99)	**CI**	87 (99)	0.73
3	**LC**	94 (99)	**CL**	86 (93)	0.53
4	**NG**	90 (99)	**GN**	90 (58)	0
5	**LD**	92 (96)	**DL**	0 (23)	1.88
6	**FP**	90 (85)	**PF**	nr	
7	**JF**	92 (98)	**FJ**	37 (10)	1.42
8	**KL**	94 (94)	**LK**	86 (99)	0.58
9	**KM**	92 (87)	**MK**	74 (99)	0.55
10	**EG**	84 (99)	**GE**	68 (28)	0.46
11	**EC**	84 (94)	**CE**	75 (85)	0.29

[a]All examples gave predominately the (S)-enantiomer.

Zn(LC) (entry 3) and its diastereomeric scaffold (BINOL)SAL **Zn(CL)** are another example in which the two catalysts have similar reactivity but a significant difference in enantioselectivity. Many catalyst pairs exhibit a drop in enantioselectivity in conjunction with a drop in reactivity for one of their diastereomers, for example, (BINOL)SAL **Zn(NG)** and (BINOL)SAL **Zn(GN)** (entry 4). In a few extreme cases, for example, (entries 5 and 6), the diastereomeric scaffold is completely ineffective. In constrast, (BINOL)SAL **Zn(JF)** and (BINOL)SAL **Zn(FJ)** (entry 7) represent a case where the change in scaffold only affects reactivity. The examples discussed above are ones for which the scaffold has a combination of $ArCH_2O$-and ArO-linkages. For most of the scaffolds containing only $ArCH_2O$-linkages, both diastereomers exhibit high reactivity and selectivity; however, there are exceptions. For example, entries 8 and 9 are among the diastereomers that exhibit rather pronounced differences in the selectivity. Diastereomeric scaffolds bearing only ArO-linkages generally differ substantially as illustrated by entries 10 and 11.

In summary, among the subunits that comprise the structures for a series of hetereobimetallic catalysts represented by **4**, the significant influence of the recognition elements (subunit IV) on reactivity and/or selectivity is perhaps the most surprising. While the observed differences are difficult to rationalize at present, much less predict, the results summarized in Figure 9 and Table 4 suggest that the zinc-bisoxazoline complex plays a structural role that goes beyond chirality directed self-assembly and beyond that of simply connecting the tethers. Instead, it seems that at least in some cases, the recognition subunit strongly influences the organization of the tethers and ligating groups and/or directly interacts with the substrate during the course of the reaction.

CONCLUSIONS

Approaches to supramolecular catalyst systems that utilize hydrogen-bonding or metal complexation directed self-assembly to organize chirality and define the topography of the chemical active site are of interest in part because such chemocatalysts are conceptually linked to biocatalysts. While significant progress has been reported toward understanding how to design and optimize catalyst performance using classical, small-molecule catalyst design motifs, much less is known on how to optimize the performance of supramolecular catalysts. An important underlying question is whether hydrogen bonding and metal complexation strategies used in the design of supramolecular catalysts offer significant advantages compared to classical approaches to asymmetric catalyst design.

One potential advantage of the supramolecular catalysts defined by structure **4** is that combinatorial methods can be employed to facilitate modular ligand/catalyst synthesis and used to probe the effectiveness of catalyst scaffold optimization. Furthermore, forming macrocyclic chelated catalysts (i.e., **4**), rather than smaller, more rigid chelates or organization through nonbonded interactions, seemingly allow for the smoother incremental variation in catalyst structure. However, as it the case with all protocols designed to effect structure optimization via a combinatorial approach, the approach is only likely to prove useful if the subunits varied combinatorially adequately explore the relevant chemical space.

In this study of structure−activity and structure-selectivity relationships of a modular supramolecular hydrogenation catalyst system, a series of BINOL phosphite derived SALs were used to prepare a series of supramolecular catalysts in situ which were evaluated in the rhodium-catalyzed asymmetric hydrogenations of two prototypical enamide substrates. The catalysts vary widely in their reactivity and enantioselectivity. Although there are exceptions, the data suggest that a balance between key elements of rigidity and flexibility is required for the successful catalysts and, moreover, that balance is required to enable effective fine-tuning via catalyst scaffold optimization. Without sufficient rigidity, subtle changes in the scaffold structure are relatively ineffective for catalyst optimization; the same holding true in cases lacking sufficient flexibility.

SALs bearing only the more flexible $ArCH_2O$-linkages are with few exceptions active and give high enantioselectivity; 58 examples of such catalysts give an average of 98% yield and 90.2% ± 3.8% ee. In contrast, those SALs bearing only more constrained ArO-linked phosphite on average give much lower lower yield and enantioselectivity under the screening conditions; 20 catalysts give an average 23% yield and 22% ee. Nearly all attempts to optimize the catalyst scaffold with SALs bearing only more constrained ArO-linked phosphite failed in comparison to the monodentate model ligand, (BINOL)POPh (**L3a**); the latter affords quantitative conversion of the product with good enantioselectivity (69−86% ee). Although it is possible that subtle electronic factors serve to differentiate the $ArCH_2O$- and ArO-linked SALs studied, it

dx.doi.org/10.1021/cs300465u | ACS Catal. 2012, 2, 2743−2752

seems more likely that the additional rotational degrees of freedom afforded to the former play a significant role in the catalyst efficiency.

Those catalysts bearing a combination of $ArCH_2O$- and ArO-linkages exhibit the widest range of performance and include the overall best performing catalyst, (BINOL)SAL **Zn(IC)**. Nonetheless, their average yield and level of enantioselectivity fall between those obtained with $ArCH_2O$-only and ArO-only catalysts; 80 catalysts bearing mixed linkages give an average 72% yield and 77% ee. Nonetheless, while the change in catalyst performance as a consequence of subltle changes in the catalyst scaffold can be quite significant, subtle changes in the empirically determined optimal scaffold structure generally have only an incremental effect.

Among the four structural subunits (recognition subunit, scaffold-generating tether subunits, ligating group subunits, and catalytic metal subunit), it is perhaps most unexpected to find that the recognition subunit can play an important role in influencing reactivity. A significant number among the pairs of diastereomeric catalysts exhibit matched/mismatched relationships. Given the structure and local symmetry (inversion symmetry) of the recognition element, we find it difficult to rationalize the matched/mismatched results solely on the basis of a remote conformational change propagated to the chiral ligating groups. Future studies will explore whether secondary interactions with the macrocyclic catalyst scaffold play an important role in determining catalyst efficiency and thereby help explain how a series of closely related supramolecular catalysts, each bearing essentially the same two BINOL-phosphite ligating groups complexed to Rh(I), exhibit such a wide range of reactivity and selectivity.

It should be emphasized that, while the findings described above may have some general applicability at a conceptual level, the specific details and trends noted above are relevant only to the specific reaction investigated (i.e., rhodium-catalyzed asymmetric hydrogenation reaction and its unique structural and mechanistic requirements); the details for other catalysts and/or reactions may and in some cases do differ.[69]

EXPERIMENTAL PROCEDURES

The following procedure is typical. To a solution of BINOL tether ((*S*,*S*)-**5I**) (3.7 mg, 5.1 μmol) and BINOL tether ((*R*,*R*)-**5C**) (3.8 mg, 5.1 μmol) in dicloromethane (DCM, 1.0 mL) was added a solution of diethyl zinc (0.10 mL, 5.6 μmol) dropwise and 3 2 mm glass beads. The resulting mixture was stirred on an orbital shaker (ca. 125 rpm) for 30 min and then concentrated in vacuo to afford (BINOL)SAL **Zn(IC)** which was diluted with dichloroethane (DCE, 2.0 mL) and used without further purification. A solution of $Rh(nbd)_2BF_4$ (1.9 mg, 5.1 μmol) in DCM (0.20 mL) was added dropwise, and the resulting mixture was stirred for 30 min at ambient temperature under N_2. A solution of *N*-(1-(4-chlorophenyl)vinyl)acetamide (**S1**) (1.0×10^2 mg, 5.1×10^2 mmol) in DCE was then added, and the vial was placed into a hydrogenated chamber. The chamber was purged with hydrogen gas (5 × 20 psi) and then pressurized to 30 psi H_2 and lightly shaken (ca. 125 rpm) at ambient temperature for 16 h. The hydrogen pressure was released, and the crude reaction mixture was concentrated and purified by flash chromatography on silica gel using EtOAc/Hexanes (1:5) as the eluent yielding (*S*)-*N*-(1-(4-chlorophenyl)ethyl)acetamide (98% yield) as a white solid: gas chromatography on a CP-Chirasil-Dex CB column (I.D. = 0.25 mm) using a temperature program of 140−200 °C at 1 °C/min) show 95% ee; $[\alpha]_D = -152$ (c = 0.5, EtOH); literature, $[\alpha]_D = -154$ (c = 0.5, EtOH, 96% ee);[70−72] ^{1}H NMR (400 MHz, $CDCl_3$) δ 7.33−7.25 (4H, m), 5.76 (1H, bs), 5.11 (1H, m), 2.00 (3H, s), 1.48 (3H, d, J = 6.92 Hz); ^{13}C NMR (100 MHz) δ 169.11, 141.79, 133.06, 128.77, 127.58, 48.20, 23.41, 21.69.

ASSOCIATED CONTENT

Supporting Information

Full asymmetric hydrogenation data table, experimental procedures, and spectral characterization of key ligands and products. This material is available free of charge via the Internet at http://pubs.acs.org.

AUTHOR INFORMATION

Corresponding Author

*Fax: +1 402-472-9402. Tel: +1 403-472-6232. E-mail: jtakacs1@unl.edu.

Present Address

†Laboratory for Specially-Promoted Research on Organocatalytic Chemistry, Graduate School of Science, Kyoto University, Kyoto, Japan.

Notes

The authors declare no competing financial interest.

ACKNOWLEDGMENTS

Acknowledgment is made to the Donors of the American Chemical Society Petroleum Research Fund for partial support of this research (PRF 47257-AC1) and to the NSF (CHE-0809637), NIH (STTR R41 GM074337), and Nebraska Research Initiative for their support. We thank Q. Zhang, K. Chaiseeda, and R. Verduzzo for some preliminary studies, and the NSF (CHE-0091975, MRI-0079750) and NIH (SIG-1-510-RR-06307) for the NMR spectrometers used in these studies carried out in facilities renovated under NIH RR016544.

REFERENCES

(1) Vineyard, B. D.; Knowles, W. S.; Sabacky, M. J.; Bachman, G. L.; Weinkauff, O. J. *J. Am. Chem. Soc.* **1977**, *99*, 5946−5952.
(2) Knowles, W. S. *Acc. Chem. Res.* **1983**, *16*, 106−112.
(3) Knowles, W. S. *Angew. Chem., Int. Ed.* **2002**, *41*, 1998−2007.
(4) Pena, D.; Minnard, A. J.; de Vries, J. G.; Feringa, B. L. *J. Am. Chem. Soc.* **2002**, *124*, 14552−14553.
(5) Reetz, M. T.; Mehler, G. *Angew. Chem., Int. Ed.* **2000**, *39*, 3889−3890.
(6) van den Berg, M.; Minnard, A. J.; Schudde, E. P.; van Esch, J.; de Vries, A. H. M.; de Vries, J. G.; Feringa, B. L. *J. Am. Chem. Soc.* **2000**, *122*, 11539−11540.
(7) Zhang, F.; Li, Y.; Li, Z. W.; He, Y. M.; Zhu, S. F.; Fan, Q. H.; Zhou, Q. L. *Chem. Commun.* **2008**, 6048−6050.
(8) Jerphagnon, T.; Bruneau, C. *Tetrahedron: Asymmetry* **2004**, *15*, 2101−2111.
(9) Breit, B. *Angew. Chem., Int. Ed.* **2005**, *44*, 6816−6825.
(10) Ringe, D.; Petsko, G. A. *Science* **2008**, *320*, 1428−1429.
(11) Carboni, S.; Gennari, S.; Pignataro, L.; Piarulli, U. *Dalton Trans.* **2011**, *40*, 4355−4373.
(12) Deuss, P. J.; den Heeten, R.; Wouter, L.; Kamer, P. C. J. *Chem.—Eur. J.* **2011**, *17*, 4680−4698.
(13) Wiester, M. J.; Ulmann, P. A.; Mirkin, C. A. *Angew. Chem., Int. Ed.* **2010**, *50*, 114−137.
(14) Gasparini, G.; Molin, M. D.; Prins, L. J. *Eur. J. Org. Chem.* **2010**, *13*, 2429−2440.
(15) van Leeuwen, P. W. N. M. *Supramolecular Catalysis*; Wiley-VCH: Weinheim, Germany, 2008.

(16) Ballester, P.; Vidal-Ferran, A.; van Leeuwen, P. W. N. M. In *Modern Strategies in Supramolecular Catalysis*; Gates, B. C., Knözinger, H., Jentoft, F., Eds.; Academic Press: New York, 2011; Advances in Catalysis; Vol. *54*, pp 63−126.
(17) Reyes, S. J.; Burgess, K. *Chem. Soc. Rev.* **2006**, *35*, 416−423.
(18) Karakhavanov, E. A.; Maksimiov, A. L.; Runova, E. A. *Russ. Chem. Rev.* **2005**, *74*, 97−111.
(19) Hofacker, A.; Parquette, J. R. *Proc. R. Soc. A.* **2010**, *466*, 1469−1487.
(20) Shao, H.; Seeifert, J.; Romano, N. C.; Helmus, J. J.; Jaroniec, C. P.; Modarelli, A.; Parquette, J. R. *Angew. Chem., Int. Ed.* **2010**, *49*, 7688−7691.
(21) Yu, J.; RajanBabu, T. V.; Parquette, J. R. *J. Am. Chem. Soc.* **2008**, *130*, 7845−7847.
(22) Mes, T.; van der Weegen, R.; Palmans, A. R. A.; Meijer, E. W. *Angew. Chem., Int. Ed.* **2011**, *50*, 5085−5089.
(23) Dong, Z.; Plampin, J. N., III; Yap, G. P. A.; Fox, J. M. *Org. Lett.* **2010**, *12*, 4002−4005.
(24) Bauer, G.; Benkő, Z.; Nuss, J.; Nieger, M.; Gudat, D. *Chem.—Eur. J.* **2010**, *16*, 12091−12095.
(25) Chikkali, S. H.; Nieger, M.; Gudat, D. *New. J. Chem.* **2010**, *34*, 1348−1354.
(26) Chikkali, S. H.; Gudat, D.; Lissner, F.; Niemeyer, M.; Schleid, T.; Nieger, M. *Chem.—Eur. J.* **2009**, *15*, 482−491.
(27) Gadzikwa, T.; Bellini, R.; Dekker, H. L.; Reek, J. N. H. *J. Am. Chem. Soc.* **2012**, *134*, 2860−2863.
(28) Bokokić, V.; Lutz, M.; Spek, A. L.; Reek, J. N. H. *Dalton Trans.* **2012**, *41*, 3740−3750.
(29) Bellini, R.; Chikkali, S. H.; Berthon-Gelloz, G.; Reek, J. N. H. *Angew. Chem., Int. Ed.* **2011**, *50*, 7342−7345.
(30) Goudriaan, P. E.; Jang, X. B.; Kuil, M.; Lemmens, R.; Van Leeuwen, P. W. N. M.; Reek, J. N. H. *Eur. J. Chem.* **2008**, 6079−6092.
(31) Jiang, X. B.; Lefort, L.; Goudriaan, P. E.; de Vries, A. H. M.; van Leeuwen, P. W. N. M.; de Vries, J. G.; Reek, J. N. H. *Angew. Chem., Int. Ed.* **2006**, *45*, 1223−1227.
(32) Van Leuuwen, P. W. N. M.; Rivillo, D.; Raynal, M.; Freixa, Z. *J. Am. Chem. Soc.* **2011**, *133*, 18562−18565.
(33) Goudriaan, P. E.; Kuil, M.; Jiang, X. B.; van Leeuwen, P. W. N. M.; Reek, J. N. H. *Dalton Trans.* **2009**, 1801−1805.
(34) Yu, L.; Wang, J.; Wu, J.; Tu, S.; Ding, K. *Angew. Chem., Int. Ed.* **2010**, *49*, 3627−3630.
(35) Patureau, F. W.; Siegler, M. A.; Spek, A. L.; Sandee, A. J.; Jugé, S.; Aziz, S.; Berkessel, A.; Reek, J. N. H. *Eur. J. Inorg. Chem.* **2012**, 496−503.
(36) Meeuwissen, J.; Sandee, A. J.; de Bruin, B.; Siegler, M. A.; Spek, A. L.; Reek, J. N. H. *Organometallics* **2010**, *29*, 2413−2421.
(37) Meeuwissen, J.; Detz, R.; Sandee, A. J.; de Bruin, B.; Siegler, M. A.; Spek, A. L.; Reek, J. N. H. *Eur. J. Inorg. Chem.* **2010**, 2992−2997.
(38) Meeuwisen, J.; Kuil, M.; van der Burg, A. M.; Sandee, A. J.; Reek, J. N. H. *Chem.—Eur. J.* **2009**, *15*, 10272−10279.
(39) Wieland, J.; Breit, B. *Nat. Chem.* **2010**, *2*, 832−837.
(40) De Greef, M.; Breit, B. *Angew. Chem., Int. Ed.* **2009**, *48*, 551−554.
(41) Laungani, A. C.; Breit, B. *Chem. Commun.* **2008**, 844−846.
(42) Kokan, Z.; Kirin, S. *RSC Adv.* **2012**, *2*, 5729−5737.
(43) Muramulla, S.; Zhao, C. G. *Tetrahedron Lett.* **2011**, *52*, 3905−3908.
(44) Li, Y.; Feng, Y.; He, Y. M.; Chen, F.; Pan, J.; Fan, Q. H. *Tetrahedron Lett.* **2008**, *49*, 2878−2881.
(45) Pignataro, L.; Boghi, M.; Civera, M.; Carboni, S.; Piarulli, U.; Gennari, C. *Chem.—Eur. J.* **2012**, *18*, 1383−1400.
(46) Pignataro, L.; Carboni, S.; Civera, M.; Colombo, R.; Piarulli, U.; Gennari, C. *Angew. Chem., Int. Ed.* **2010**, *49*, 6633−6637.
(47) Ohmatsu, K.; Ito, M.; Kunienda, T.; Ooi, T. *Nat. Chem.* **2012**, *4*, 473−477.
(48) Brown, J. M.; Deeth, R. J. *Angew. Chem., Int. Ed.* **2009**, *48*, 4476−4479 , and references cited therein.
(49) Knowles, R. R.; Jacobsen, E. N. *Proc. Natl. Acad. Sci. U.S.A.* **2010**, *107*, 20678−20685.
(50) Wieland, J.; Breit, B. *Nat. Chem.* **2010**, *2*, 832−837.
(51) Meeuwissen, J.; Reek, J. N. H. *Nat. Chem.* **2010**, *2*, 615−621.
(52) Takacs, J. M.; Reddy, D. S.; Moteki, S. A.; Wu, D.; Palencia, H. *J. Am. Chem. Soc.* **2004**, *126*, 4494−4495.
(53) Moteki, S. A.; Takacs, J. M. *Angew. Chem., Int. Ed.* **2008**, *47*, 894−897.
(54) Moteki, S. A.; Toyama, K.; Liu, Z.; Ma, J.; Holmes, A.; Takacs, J. M. *Chem. Commun.* **2012**, *48*, 263−265.
(55) Takacs, J. M.; Hrvatin, P. M.; Atkins, J. M.; Reddy, D. S.; Clark, J. L. *New. J. Chem.* **2005**, *29*, 263−265.
(56) Atkins, J. M.; Reddy, D. S.; Moteki, S. A.; DiMagno, S. G.; Takacs, J. M. *Org. Lett.* **2006**, *8*, 2759−2762.
(57) In the present context, ^{S}T and ^{R}T in SAL (^{S}T^{R}T) each represent one from among tethers A−P for the (S,S)-**5** and (R,R)-**5** box derivatives, respectively.
(58) Takacs, J. M.; Chaiseeda, K.; Moteki, S. A.; Reddy, D. S.; Wu, D.; Chandra, K. *Pure Appl. Chem.* **2006**, *78*, 501−509.
(59) Drexler, H. J.; You, J.; Zhang, S.; Fischer, C.; Baumann, W.; Spannenberg, A.; Heller, D. *Org. Process Res. Dev.* **2003**, *7*, 355−361.
(60) Alternative catalyst precursors, e.g., $Rh(cod)_2BF_4$, $Rh(cod)_2SbF_6$, $Rh(cod)_2OTf$, give similar results under these reactions conditions.
(61) Reetz, M. T.; Sell, T.; Meiswinkel, A.; Mehler, G. *Angew. Chem., Int. Ed.* **2003**, *42*, 790−793.
(62) Reetz, M. T.; Fu, Y.; Meiswinkel, A. *Angew. Chem., Int. Ed.* **2006**, *45*, 1412−1415.
(63) Reetz, M. T.; Mehler, G.; Bondarev, O. *Chem. Commun.* **2006**, 2292−2294.
(64) Note that tether subunits A, B, and H were largely omitted from the set of SALs screened in this study.
(65) Reetz, M. T. *Angew. Chem., Int. Ed.* **2008**, *47*, 2556−2588.
(66) As a side note, we find a similar trend in other reactions using these or other similar supramolecular catalysts.
(67) The yellow data points in Graph A are for catalysts that incorporate only tethers C−G, the blue only I−P, and the green are for mixed combinations of (C−G) and (I−P).
(68) After much initial controversy, a similar balance is now generally accepted in enzymatic catalysts. For example, see: Koshland, D. E. *Nature* **2004**, *4323*, 447.
(69) For example, the SALs and catalysts bearing aryloxy-linkages are the empirically determined preferred motif in the rhodium-catalyzed asymmetric hydroboration of substituted styrenes with pinacolborane; see ref 49.
(70) Zhang, Q.; Takacs, J. M. *Org. Lett.* **2008**, *10*, 545−548.
(71) Burk, M. J.; Wang, Y. M.; Lee, J. R. *J. Am. Chem. Soc.* **1996**, *118*, 5142−5143.
(72) Zhu, G.; Casalnuovo, A. L.; Zhang, X. *J. Org. Chem.* **1998**, *63*, 8100−8101.